RESEARCH ARTICLE

Effective Photosensitization in Excited-State Equilibrium: Brilliant Luminescence of Tb^{III} Coordination Polymers Through Ancillary Ligand Modifications

Yuichi Kitagawa,*[a-b] Ryoma Moriake,[c] Tomoko Akama,[b,d] Koki Saito,[c] Kota Aikawa,[c] Sunao Shoji,[a-b] Koji Fushimi,[a] Masato Kobayashi,[b,d] Tetsuya Taketsugu,[b,d] and Yasuchika Hasegawa*[a-b]

[a] Dr. Yuichi Kitagawa, Dr. Sunao Shoji, Dr. Koji Fushimi, Prof. Yasuchika Hasegawa
Faculty of Engineering, Hokkaido University, Kita 13, Nishi 8, Kita-ku Sapporo, Hokkaido 060-8628, Japan.
E-mail: y-kitagawa@eng.hokudai.ac.jp; hasegaway@eng.hokudai.ac.jp
[b] Dr. Yuichi Kitagawa, Dr. Tomoko Akama, Dr. Sunao Shoji, Dr. Masato Kobayashi, Prof. Tetsuya Taketsugu, Prof. Yasuchika Hasegawa
Institute for Chemical Reaction Design and Discovery (WPI-ICReDD), Hokkaido University, Kita 21, Nishi 10, Kita-ku, Sapporo, Hokkaido 001-0021, Japan.
[c] Mr. Ryoma Moriake, Mr. Koki Saitou, Mr. Kota Aikawa
Graduate School of Chemical Sciences and Engineering Hokkaido University, Kita 13, Nishi 8, Kita-ku, Sapporo, Hokkaido, 060-8628, Japan.
[d] Dr. Tomoko Akama, Dr. Masato Kobayashi, Prof. Tetsuya Taketsugu
Faculty of Science, Hokkaido University, Kita 10, Nishi 8, Kita-ku, Sapporo, Hokkaido, 060-0810, Japan.

Supporting information for this article is given via a link at the end of the document.

Abstract: Molecular photosensitizers provide efficient light-absorbing abilities for photo-functional materials. Herein, effective photosensitization in excited-state equilibrium is demonstrated using five Tb^{III} coordination polymers. The coordination polymers are composed of Tb^{III} ions (emission center), hexafluoroacetylacetonato (photosensitizer ligands), and phosphine oxide-based bridges (ancillary ligands). The two types of ligand combinations induces a rigid coordination structure via intermolecular interactions, resulting in high thermal stability (with decomposition temperatures above 300 °C). Excited-triplet-state lifetimes of photosensitizer ligands (τ = 120 – 1320 μs) are strongly dependent on the structure of the ancillary ligands. The photosensitizer with a long excited-triplet-state lifetime (τ ≥ 1120 μs) controls the excited state equilibrium between the photosensitizer and Tb^{III}, allowing the construction of Tb^{III} coordination polymer with high Tb^{III} emission quantum yield (≥ 70%).

Introduction

Molecular photosensitizers provide efficient light-absorbing abilities for photo-functional materials (e.g., photocatalysts[1], organic solar cells[2], and luminophores[3]). The photosensitization system includes forward and reverse energy-transfer processes in the excited state. The suppression of reverse energy-transfer is a key factor for efficient photo-sensitization. Among the various photo-sensitization system, luminescent lanthanide complexes with long emission lifetimes have been actively studied to understand the reverse energy transfer process.[4-9]

In the photosensitized lanthanide luminescence, the organic ligands undergo intersystem crossing from the lowest singlet excited state (S_1) to the lowest triplet excited state (T_1) after excitation, thereby transferring their absorbed energy to the Ln^{III} ion.[10] In 1970, Sato and coworkers demonstrated the importance of the T_1 state for energy transfer to the $^5D_1$ level in Eu^{III} complexes with β-diketonate ligands.[11] They showed that the emission quantum yield due to ligand excitation was maximum when the T_1 level was ~1200 cm^{-1} above the $^5D_1$ level. Sabbatini and Ziessel found the formation of the excited-state equilibration between T_1 and Ln^{III} emitting states in case of a small energy gap.[12] The excited-state equilibrium systems have been demonstrated using the various typed ligands by Parker and Faulkner.[13-17] Recently, we demonstrated that a poly-aromatic hydrocarbon photosensitizer with a long-lived T_1 state provides the strong emission in the excited state equilibrium (Fig. 1a-b).[18,19] Herein, we provide a novel method for controlling the T_1 lifetime of photosensitizer units by changing the structure of the ancillary ligand of the complex (Fig. 1c). The present method, which leaves the photosensitizer unmodified, opens up new possibilities for the development of photofunctional materials.

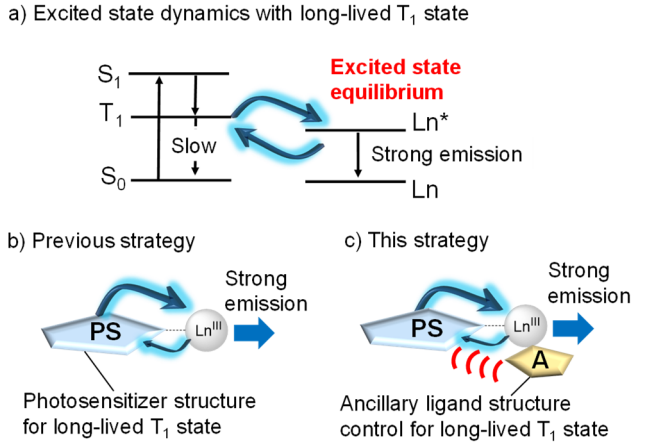

Figure 1. (a) Excited state dynamics with long-lived T_1 state. (b) Previous strategy: Photosensitizer structures altered for long-lived T_1 state (PS: photosensitizer). (c) This strategy: Ancillary ligand altered for long-lived T_1 state (A: ancillary ligand).

To demonstrate this concept, we designed Tb^{III} coordination polymers with hexafluoroacetylacetonate (hfa) and phosphine oxide ligands (Fig. 2a). The hfa ligand (T_1 ≈ 22,000 cm^{-1}) is well-known for inducing effective reverse energy transfer from Tb^{III} ion (Emitting level ($^5D_4$): 20,500 cm^{-1}).[20] In a previous report, Tb^{III}

coordination polymers with bidentate phosphine oxide linkers allow the effective modulation of the hfa excited state based on the long-range interaction.[21] To evaluate the effect of hfa on the photosensitization process, three benzene-typed linkers with high T_1 level (≥ 24,600 cm^{-1})[22] were selected to suppress the formation of excited state in the linkers (Fig. 2b).

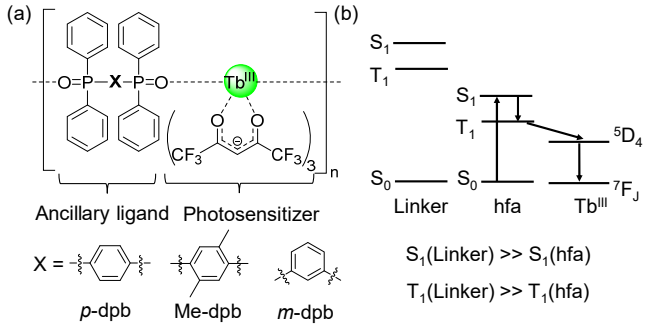

Figure 2. (a) Molecular design of Tb^{III} coordination polymers and (b) their energy diagrams.

Results and Discussion

The single crystals of three coordination polymers were obtained by recrystallization from methanol. The crystal structures are shown in Fig. 3 and Table S1. The coordination site of the Tb^{III} polymer unit comprises three hfa ligands and one phosphine oxide linker. Intermolecular CH–F interactions (2.5–2.9 Å) between the hfa ligand and the phosphine oxide ligand were observed. The decomposition temperature of Tb^{III} coordination polymers was found to be above 300 °C (Figure S1), which is caused by the effective intermolecular interactions.

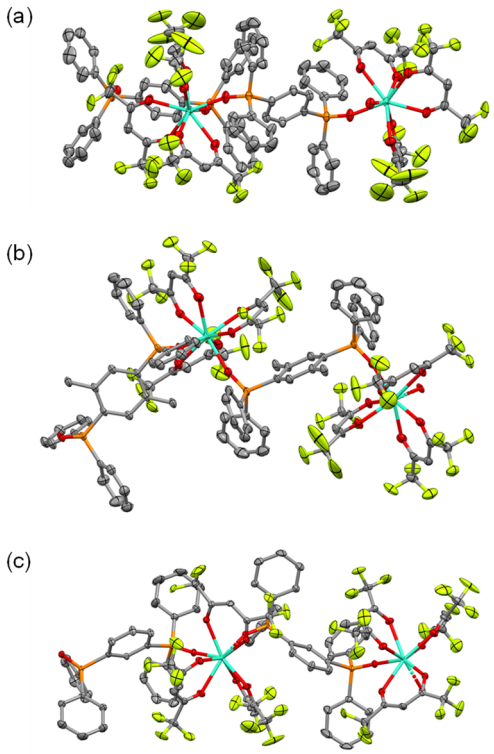

Figure 3. ORTEP drawings (ellipsoids set at 50% probability) of (a) $[Tb(hfa)_3(p\text{-dpb})]_n$,[21] (b) $[Tb(hfa)_3(Me\text{-dpb})]_n$, and (c) $[Tb(hfa)_3(m\text{-dpb})]_n$.

To clarify the coordination geometry of the unit, we performed continuous shape measure (CShM) analysis.[23] The continuous shape measure factor, *S,* was calculated to estimate the degree of distortion of the coordination structure using crystal structure data. Based on the CShM analysis, the polyhedron structures of the units in $[Tb(hfa)_3(p\text{-dpb})]_n$ were classified as the square antiprism structures. On the other hand, $[Tb(hfa)_3(Me\text{-dpb})]_n$ and $[Tb(hfa)_3(m\text{-dpb})]_n$ are categorized as trigonal dodecahedron structure (Table S2).

The emission spectra of $[Tb(hfa)_3(p\text{-dpb})]_n$, $[Tb(hfa)_3(Me\text{-dpb})]_n$, and $[Tb(hfa)_3(m\text{-dpb})]_n$ are shown in Fig. 4. The emission peaks of the three Tb^{III} coordination polymers at approximately 490, 550, 580, 620, and 650 nm were assigned to the $^5D_4 \rightarrow {}^7F_6$, $^5D_4 \rightarrow {}^7F_5$, $^5D_4 \rightarrow {}^7F_4$, $^5D_4 \rightarrow {}^7F_3$, and $^5D_4 \rightarrow {}^7F_2$ transitions, respectively. The respective excitation spectra showed a strong signal in UV region, indicating the occurrence of energy transfer from the hfa ligands to the Tb^{III} ions.

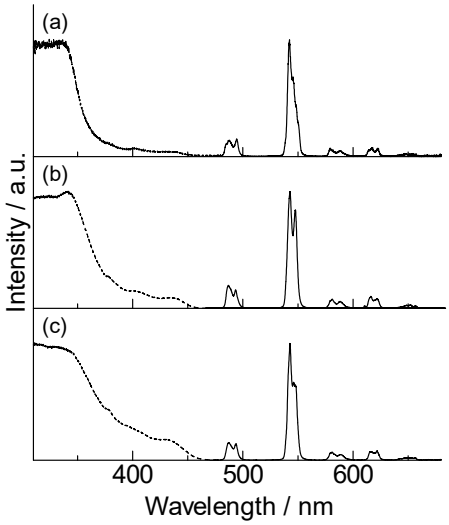

Figure 4. Emission and excitation spectra of (a)$[Tb(hfa)_3(p\text{-dpb})]_n$, (b) $[Tb(hfa)_3(Me\text{-dpb})]_n$, and (c) $[Tb(hfa)_3(m\text{-dpb})]_n$ in the solid state (λ_{ex} = 370 nm, λ_{em} = 542 nm). Normalized by intensity maxima.

Table 1. Photophysical properties of Tb^{III} coordination polymers in the solid state.

	τ / μs	τ / μs	Φ / %	Emitting level / cm^{-1}
$[Tb(hfa)_3(p\text{-dpb})]_n$	70.0[a]	67.0[c]	6.2[d]	20,500
$[Tb(hfa)_3(Me\text{-dpb})]_n$	720[a]	460[c]	54[d]	20,500
$[Tb(hfa)_3(m\text{-dpb})]_n$	680[a]	410[c]	80[d]	20,500
$[Gd(hfa)_3(p\text{-dpb})]_n$	120 [b]	-	-	22,400[e]
$[Gd(hfa)_3(Me\text{-dpb})]_n$	370[b]	-	-	22,100[e]
$[Gd(hfa)_3(m\text{-dpb})]_n$	1130[b]	-	-	21,700[e]

[a] λ_{ex} = 355 nm, λ_{em} = 540 nm under vacuum condition [b] λ_{ex} = 355 nm, λ_{em} = 450 nm under vacuum condition. [c] λ_{ex} = 355 nm, λ_{em} = 540 nm under air [d] λ_{ex} = 370 nm under Ar condition. [e] Energy levels are estimated by phosphorescence spectra (Figure S11).

The emission quantum yields (Φ) and emission lifetimes (τ) are summarized in Table 1. The emission quantum yield of $[Tb(hfa)_3(m\text{-dpb})]_n$ (80%) was the highest, followed by those of $[Tb(hfa)_3(Me\text{-dpb})]_n$ (54%) and $[Tb(hfa)_3(p\text{-dpb})]_n$ (6.2%). The emission lifetime of $[Tb(hfa)_3(p\text{-dpb})]_n$ (τ = 70 μs) is much shorter than those of $[Tb(hfa)_3(Me\text{-dpb})]_n$ (τ = 720 μs) and $[Tb(hfa)_3(m\text{-dpb})]_n$ (τ = 680 μs). To confirm the formation of the excited state equilibrium between the $^5D_4$ (Tb) and T_1 (hfa) states, oxygen-dependent emission decays were estimated for the Tb^{III} coordination polymers (Figure S9). The observed oxygen-dependent emission lifetimes (Table 1) revealed the formation of an excited state equilibrium in $[Tb(hfa)_3(Me\text{-dpb})]_n$ and $[Tb(hfa)_3(m\text{-dpb})]_n$.

The phosphorescence spectra of the Gd^{III} coordination polymers were measured to evaluate their T_1 energy levels and lifetimes (Figure S11).[21] The estimated T_1 levels that originate from hfa excited states are almost the same for three coordination polymers (Table 1). The quantum chemical calculations also show almost the same T_1 levels for Tb^{III} coordination polymers (Table S5). The emission lifetime of $[Gd(hfa)_3(m\text{-dpb})]_n$ (1130 μs) is much longer than those of $[Gd(hfa)_3(Me\text{-dpb})]_n$ (370 μs) and $[Gd(hfa)_3(p\text{-dpb})]_n$ (120 μs). We propose that the T_1 lifetimes are related to the photosensitized emission quantum yields for the present Tb^{III} coordination polymers.

To understand the electronic structure of T_1 states in the hfa ligands, temperature-dependent emission analyses of the Gd^{III} coordination polymers were also performed (Figure S12). These results indicate that the T_1 lifetimes are dependent on the non-radiative rate constants of the coordination polymers ($[Gd(hfa)_3(p\text{-dpb})]_n$: 8,300 s^{-1}, $[Gd(hfa)_3(Me\text{-dpb})]_n$: 2,400 s^{-1}, $[Gd(hfa)_3(m\text{-dpb})]_n$: 830 s^{-1}). The small non-radiative rate in $[Gd(hfa)_3(m\text{-dpb})]_n$ is closely related to the highest emission quantum yield of $[Tb(hfa)_3(m\text{-dpb})]_n$. Overall, our experimental results demonstrate that the ancillary ligands strongly affect the excited state lifetime of photosensitizer, resulting in efficient photosensitization in the excited-state equilibrium, although the detailed non-radiative pathway is unclear at the present stage (See Supplementary Information).

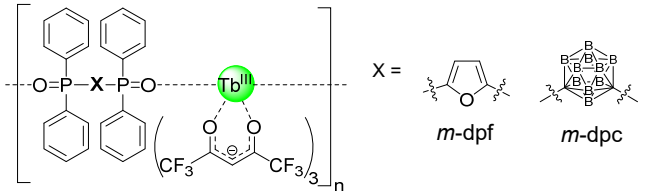

Figure 5. Tb^{III} coordination polymers with furan ($[Tb(hfa)_3(m\text{-dpf})]_n$) and carborane ($[Tb(hfa)_3(m\text{-dpc})]_n$) frameworks.

To expand our model, the linker framework in the phosphine oxide ligands was changed from benzene to furan[24] and carborane[25] (Fig. 5).[26] The crystal structures are shown in Fig. 6 and Table S6. The coordination site of the Tb^{III} polymer unit comprises three hfa ligands and one phosphine oxide linker. The emission spectra of $[Tb(hfa)_3(m\text{-dpf})]_n$ and $[Tb(hfa)_3(m\text{-dpc})]_n$ and excitation are shown in Fig. 7. These spectra are similar to those of Tb^{III} coordination polymer with benzene-typed linkers (Fig. 4). The photophysical parameters for the coordination polymers are summarized in Table 2. These coordination polymers have also shown a good correlation between the T_1 lifetimes and emission quantum yields. In particular, a high emission quantum yield was observed for novel Tb^{III} coordination polymer with carborane framework (Φ = 88%).

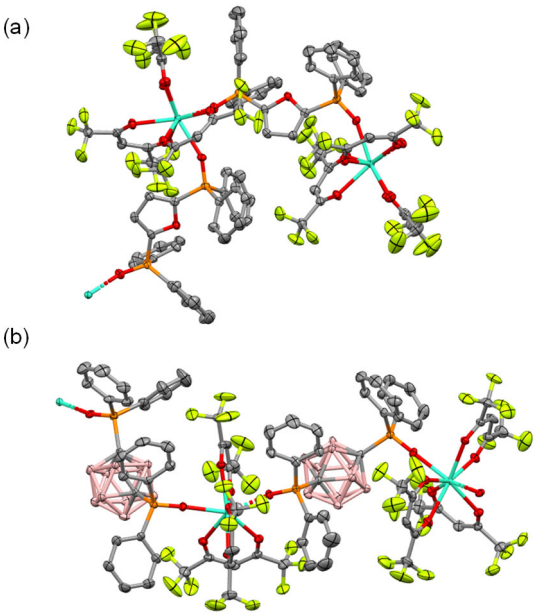

Figure 6. ORTEP drawings (ellipsoids set at 50% probability) of (a) $[Tb(hfa)_3(m\text{-dpf})]_n$[24] and (b) $[Tb(hfa)_3(m\text{-dpc})]_n$.

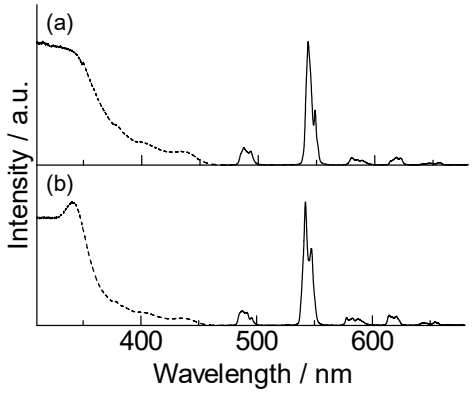

Figure 7. Emission and excitation spectra of (a) $[Tb(hfa)_3(m\text{-dpf})]_n$ and (b) $[Tb(hfa)_3(m\text{-dpc})]_n$ in the solid state. Normalized by intensity maxima.

Table 2. Photophysical properties of Tb^{III} and Gd^{III} coordination polymers in the solid state.

	τ / μs	τ / μs	Φ / %	Emitting level / cm^{-1}
$[Tb(hfa)_3(m\text{-dpf})]_n$	640[a]	360[c]	70[d]	20,500
$[Tb(hfa)_3(m\text{-dpc})]_n$	690[a]	430[c]	88[d]	20,500
$[Gd(hfa)_3(m\text{-dpf})]_n$	1120[b]	-	-	21,800[e]
$[Gd(hfa)_3(m\text{-dpc})]_n$	1320[b]	-	-	21,800[e]

[a] λ_{ex} = 355 nm, λ_{em} = 540 nm under vacuum condition. [b] λ_{ex} = 355 nm, λ_{em} = 450 nm under vacuum condition. [c] λ_{ex} = 355 nm, λ_{em} = 540 nm under air condition. [d] λ_{ex} = 370 nm under Ar condition. [e] Energy levels are estimated by phosphorescence spectra (Figure S16).

Conclusion

In this study, the effective photosensitization model with excited-state equilibrium was developed using Tb^{III} coordination polymers. The non-radiative rate pathway of the photosensitizer unit strongly depended on the ancillary ligands of the coordination polymers, indicating that these ligands controlled the photosensitization efficiency. These results provide new insights in photosensitizer design for improving photo-functional materials.

Experimental Section

General methods: NMR spectra were recorded on a JEOL ECS-400 spectrometer (^{1}H: 400 MHz). Tetramethylsilane (δ = 0.00 ppm for ^{1}H NMR) was employed as internal standards. Electrospray ionization mass spectrometry (ESI-MS) was performed using JEOL JMS-T100 LP instrument. Elemental analyses were performed using MICRO CORDER JM10. Emission spectra and excitation spectra for Tb^{III} and Gd^{III} coordination polymers were measured using a Horiba Fluorolog®-3 spectrofluorometer and FP-6600 with a cryostat (Thermal Block Company, SA-SB245T), respectively. Emission lifetimes were measured using a Nd-YAG laser with a cryostat (Thermal Block Company, SA-SB245T). The photosensitized emission quantum yields (excitation wavelength: 370 nm) for the Tb^{III} coordination polymer (powder sample) were obtained using a JASCO F-6300-H spectrometer attached to a JASCO ILF-533 integrating sphere unit (φ = 100 mm) under Ar condition. The wavelength dependence of the detector response and beam intensity of the Xe light source for each spectrum were calibrated using a standard light source.

Materials: *n*-BuLi (1.6 mol/L in *n*-hexane) was purchased from Kanto Chemical Co., Inc. Hexafluoroacetylacetone (>95.0 %), 1,3-dibromobenzene (>97.0 %), 1,4-dibromobenzene (>99.0 %), 2,5-dibromo-*p*-xylene (>98.0 %), 2,5-dibromofuran, and chlorodiphenylphosphine (>97.0 %) were obtained from Tokyo Chemical Industry Co., Ltd. Terbium acetate hexahydrate (99.9+%), gadolinium acetate tetrahydrate (99.9+%), *m*-carborane (96+%), and hydrogen peroxide were purchased from Fujifilm Wako.

Preparation of 1,4-bis(diphenylphosphoryl)benzene (*p*-dpb): We prepared the *p*-dpb ligand according to previous our method.[21]

Preparation of 1,4-dimethyl-2,5-bis(diphenylphosphoryl)benzene (Me-dpb): A solution of *n*-BuLi (40 mL, 1.6 M in *n*-hexane) was added to a solution of 2,5-dibromo-*p*-xylene (5.0 g, 18.9 mmol) in dry THF (15 mL) at −78 °C under Ar atmosphere. The mixture was stirred for 2 h, after which chlorodiphenylphosphine (7.0 mL, 39.0 mmol) was added to the solution at −78 °C. The mixture was gradually heated to room temperature and stirred for 14 h. After the reaction, the solution was added dichloromethane and washed with brine. The solvent was evaporated, and the solid powder was dissolved in dichloromethane (20 mL). The solution was cooled to 0 °C and added an aqueous solution of H_2O_2 (30 %, 5 mL). The mixture was then stirred for 2 h. The organic layer was separated, washed with brine and dried over $MgSO_4$. The solvent was evaporated, and the resultant residue was purified by silica gel column chromatography (methanol/ethyl acetate = 5/95). The obtained powder was re-precipitated from ethyl acetate to give the product as a white powder.
Yield: 10% (0.96 g, 1.89 mmol), ^{1}H NMR (400 MHz, $CDCl_3$): δ 7.66-7.46 (m, 20H), 6.98-6.89 (dd, *J* = 13.6, 4.0 Hz, 2H), 2.29-2.24 (s, 6H) ppm. ESI-MS: m/z calcd. for $C_{32}H_{29}O_2P_2$ $[M+H]^+$ = 507.16; found: 507.16.

Preparation of 1,3-bis(diphenylphosphoryl)benzene (*m*-dpb): A solution of *n*-BuLi (20 mL, 1.6 M in *n*-hexane) was added to a solution of 1,3-dibromobenzene (3.14 g, 13.3 mmol) in dry THF (15 mL) at −78 °C under Ar atmosphere. The mixture was stirred for 2 h, after which chlorodiphenylphosphine (5.5 mL, 31 mmol) was added to the solution at −78 °C. The mixture was gradually heated to room temperature and stirred for 14 h. After the reaction, the solution was added dichloromethane and washed with brine. The solvent was evaporated, and the solid powder was dissolved in dichloromethane (15 mL). The solution was cooled to 0 °C and added an aqueous solution of H_2O_2 (30 %, 4 mL). The mixture was then stirred for 2 h. The organic layer was separated, washed with brine and dried over $MgSO_4$. The solvent was evaporated, and the resultant residue was purified by silica gel column chromatography (methanol/ethyl acetate = 5/95). The obtained powder was re-precipitated from ethyl acetate to give the product as a white powder.
Yield: 18% (1.17 g, 2.4 mmol), ^{1}H NMR (400 MHz, $CDCl_3$) δ 7.98-7.93 (m, 2H), 7.71 (t, *J* = 11.6 Hz, 1H), 7.63-7.51 (m, 13H), 7.44-7.39 (m, 8H). ESI-MS: m/z calcd. for $C_{30}H_{24}NaO_2P_2$ $[M+Na]^+$ = 501.44; found: 501.10.

Preparation of 2,5-bis(diphenylphosphoryl)furan (*m*-dpf): We prepared the *m*-dpf ligand according to previous our method.[24]

Preparation of 2,5-bis(diphenylphosphoryl)carborane (*m*-dpc): A solution of *n*-BuLi (3.0 mL, 1.6 M in *n*-hexane) was added to a solution of *m*-carborane (0.30 g, 2.08 mmol) in dry diethyl ether (10 mL) at −78 °C under Ar atmosphere. The mixture was stirred for 0.5 h, after which a chlorodiphenylphosphine (0.95 mL, 5.1 mmol) was added to the solution at −78 °C, and stirred for 2 h. After the reaction, the mixture was washed with water. The solution was evaporated, and the solid powder was dissolved in THF (5 mL). The solution was cooled to 0 °C and added an aqueous solution of H_2O_2 (30 %, 3 mL). The mixture was stirred for 4 h. The solution was added dichloromethane, and washed with brine. The solvent was evaporated, and the resultant residue was purified by silica gel column chromatography (methanol/ethyl acetate = 5/95). The obtained powder was re-precipitated from ethyl acetate to give the product as a white powder.
Yield: 43% (0.49 g, 0.89 mmol), ^{1}H NMR ($CDCl_3$, 400 MHz) δ 7.89-7.94 (m, 8H), 7.59-7.55 (m, 4H), 7.51-7.45 (m, 8H), 3.49-1.20 (m, 10H), MS(ESI): m/z calcd. for $C_{26}H_{31}B_{10}P_2O_2$ $[M+H]^+$ = 547.27 ; found = 547.26

Preparation of $[Tb(hfa)_3(p\text{-dpb})]_n$
We prepared the $[Tb(hfa)_3(p\text{-dpb})]_n$ according to previous our method.[21]
Elemental analysis calcd (%) for$[Tb(hfa)_3(p\text{-dpb})]_n$: C, 42.95; H, 2.16. Found C, 43.02; H, 1.98.

Preparation of $[Gd(hfa)_3(p\text{-dpb})]_n$
We prepared the $[Gd(hfa)_3(p\text{-dpb})]_n$ according to previous our method.[21]
Elemental analysis calcd (%) for $[Gd(hfa)_3(p\text{-dpb})]_n$: C, 43.00; H, 2.17. Found C, 42.85; H, 2.02.

Preparation of $[Tb(hfa)_3(Me\text{-dpb})]_n$
$[Tb(hfa)_3(H_2O)_2]$ (165 mg, 0.2 mmol) and Me-dpb (101 mg, 0.2 mmol) were dissolved in methanol (15 mL). The solution was refluxed with stirring for 1 h to yield a white precipitate. The precipitate was then filtered and washed several times with methanol, dichloromethane, and hexane. The obtained powder was recrystallization from methanol to afford a white crystal.
Yield: 27% (0.070 g, 0.054 mmol), ESI-MS: m/z calcd. for $[Tb_2(hfa)_5(Me\text{-}dpb)_3]^+$ = 2871.26; found: 2871.38. Elemental analysis calcd (%) for $[Tb(hfa)_3(Me\text{-dpb})]$: C, 43.88; H, 2.43. Found C, 43.91; H, 2.25.

Preparation of $[Gd(hfa)_3(Me\text{-dpb})_n]$
$[Gd(hfa)_3(H_2O)_2]$ (165 mg, 0.2 mmol) and Me-dpb (101 mg, 0.2 mmol) were dissolved in methanol (15 mL). The solution was refluxed with stirring for 1 h to yield a white precipitate. The precipitate was then filtered and washed several times with methanol, dichloromethane, and hexane. The obtained powder was recrystallization from methanol to afford a white crystal.
Yield: 30% (0.078 g, 0.061 mmol), ESI-MS: m/z calcd. for $[Gd_2(hfa)_5(Me\text{-}dpb)_3]^+$ = 2869.29; found: 2869.20. Elemental analysis calcd (%) for $[Gd(hfa)_3(Me\text{-dpb})]$: C, 43.93; H, 2.43. Found C, 43.69; H, 2.27.

Preparation of $[Tb(hfa)_3(m\text{-dpb})]_n$

$[Tb(hfa)_3(H_2O)_2]$ (185 mg, 0.23 mmol) and *m*-dpb (105 mg, 0.22 mmol) were dissolved in methanol (15 mL). The solution was refluxed with stirring for 1 h to yield a white precipitate. The precipitate was then filtered and washed several times with methanol, dichloromethane, and hexane. The obtained powder was recrystallization from methanol to afford a white crystal.
Yield: 48% (0.139 g, 0.11 mmol), ESI-MS: m/z calcd. for $[Tb_2(hfa)_5(m\text{-}dpb)_3]^+$ = 2788.48; found: 2788.18. Elemental analysis calcd (%) for $[Tb(hfa)_3(m\text{-}dpb)]$: C, 42.95; H, 2.16. Found C, 42.76; H, 2.01.

Preparation of $[Gd(hfa)_3(m\text{-}dpb)]_n$
$[Gd(hfa)_3(H_2O)_2]$ (172 mg, 0.21 mmol) and *m*-dpb (108 mg, 0.23 mmol) were dissolved in methanol (15 mL). The solution was refluxed with stirring for 1 h to yield a white precipitate. The precipitate was then filtered and washed several times with methanol, dichloromethane, and hexane. The obtained powder was recrystallization from methanol to afford a white crystal.
Yield: 49% (0.132 g, 0.1 mmol), ESI-MS: m/z calcd. for $[Gd_2(hfa)_5(m\text{-}dpb)_3]^+$ = 2785.20; found: 2785.18. Elemental analysis calcd (%) for $[Gd(hfa)_3(m\text{-}dpb)]$: C, 43.00; H, 2.17. Found C, 42.85; H, 2.02.

Preparation of $[Tb(hfa)_3(m\text{-}dpf)]_n$
We prepared the $[Tb(hfa)_3(m\text{-}dpf)]_n$ according to previous our method.[24]
Elemental analysis calcd (%) for $[Tb(hfa)_3(p\text{-}dpf)]_n$: C, 42.37; H, 2.02. Found C, 41.47; H, 1.86.

Preparation of $[Gd(hfa)_3(m\text{-}dpf)_n]$
We prepared the $[Gd(hfa)_3(m\text{-}dpf)]_n$ according to previous our method.[24]
Elemental analysis calcd (%) for $[Gd(hfa)_3(m\text{-}dpf)]_n$: C, 41.42; H, 2.02. Found C, 41.27; H, 1.80.

Preparation of $[Tb(hfa)_3(m\text{-}dpc)]_n$
$[Tb(hfa)_3(H_2O)_2]$ (390 mg, 0.48 mmol) and *m*-dpc (200 mg, 0.37 mmol) were dissolved in toluene (30 mL). The solution was refluxed with stirring for 6 h. After the reaction, the solution was cooled to room temperature and the solvent was evaporated. The residual solid was dissolved in 1,4-dioxane, and the solution was refluxed for 2h. The mixture was cooled to room temperature. The precipitate was filtered and washed several times with methanol, dichloromethane, and hexane. The product was recrystallization from methanol to afford a white crystal.
Yield: 72% (0.353 g, 0.27 mmol), MS (ESI): *m*/*z* calcd for $C_{41}H_{33}B_{10}TbF_{18}O_8P_2$; $[M–hfa]^+$ = 1117.17, found = 1117.17, $[2M–hfa]^+$ = 2441.34, found = 2441.28, Elemental analysis calculated (%) for $[Tb(hfa)_3(m\text{-}dpc)]$: C, 37.18, H, 2.52, found : C, 37.17, H, 2.52.

Preparation of $[Gd(hfa)_3(m\text{-}dpc)]_n$
$[Gd(hfa)_3(H_2O)_2]$ (500 mg, 0.61 mmol) and *m*-dpc (300 mg, 0.55 mmol) were dissolved in toluene (30 mL). The solution was refluxed with stirring for 6 h. After the reaction, the solution was cooled to room temperature and the solvent was evaporated. The residual solid was dissolved in 1,4-dioxane, and the solution is refluxed for 2 h. The mixture was cooled to room temperature. The precipitate was then filtered and washed several times with methanol, dichloromethane, and hexane. The product was recrystallization from methanol to afford a white crystal.
Yield: 80% (0.65 g, 0.49 mmol), MS (ESI): *m*/*z* calculated for $C_{41}H_{33}B_{10}GdF_{18}O_8P_2$; $[M–hfa]^+$ = 1346.15, found = 1346.18.

Single-Crystal X-ray Structure Determination: Single crystals of the $[Tb(hfa)_3(Me\text{-}dpb)]_n$, $[Tb(hfa)_3(m\text{-}dpb)]_n$, and $[Tb(hfa)_3(m\text{-}dpc)]_n$ were mounted on micromesh (MiTeGen M3-L19–25L) using paraffin oil. Measurements were made by using a Rigaku RAXIS RAPID imaging-plate area detector or XtaLAB AFC11 (RCD3) with graphite-monochromated Mo-K_α radiation. Non-hydrogen atoms were anisotropically refined. All calculations were performed using a crystal-structure crystallographic software package. The CIF data were confirmed by the check CIF/PLATON service. Deposition Number(s) 2150409 (for $[Tb(hfa)_3(Me\text{-}dpb)]_n$), 2151433 (for $[Tb(hfa)_3(m\text{-}dpb)]_n$), and 2150410 (for $[Tb(hfa)_3(m\text{-}dpc)]_n$) contain(s) the supplementary crystallographic data for this paper. These data are provided free of charge by the joint Cambridge Crystallographic Data Centre and Fachinformationszentrum Karlsruhe Access Structures service www.ccdc.cam.ac.uk/structures.

Acknowledgements

This work was partially supported by grant-in-aid for grant numbers JP20H02748, JP20H04653, JP20H05197, JP20K21201, and JP21K18969. We are particularly grateful for experimental assistance by Prof. H. Ito and Dr. J. Mingoo of Hokkaido University. This work was also supported by the Institute for Chemical Reaction Design and Discovery (ICReDD), established by the World Premier International Research Initiative (WPI) of MEXT, Japan.

Keywords: Energy transfer• Luminescence • Photosensitizer • Terbium • Triplet state

[1] Y. Yamazaki, H. Takeda and O. Ishitani, *J. Photochem. Photobiol., C* **2015**, *25*, 106-137.
[2] L. L. Li and E. W. Diau, *Chem. Soc. Rev.* **2013**, *42*, 291-304.
[3] J.-C. G. Bünzli and C. Piguet, *Chem. Soc. Rev.* **2005**, *34*, 1048-1077.
[4] N. M. Shavaleev, S. V. Eliseeva, R. Scopelliti and J.-C. G. Bünzli, *Inorg. Chem.* **2010**, *49*, 3927-3936.
[5] N. M. Shavaleev, S. V. Eliseeva, R. Scopelliti and J.-C. G. Bünzli, *Chem. – Eur. J.* **2009**, *15*, 10790-10802.
[6] S. Omagari, T. Nakanishi, Y. Kitagawa, T. Seki, K. Fushimi, H. Ito, A. Meijerink and Y. Hasegawa, *Sci. Rep.* **2016**, *6*, 37008.
[7] A. M. Kaczmarek, Y.-Y. Liu, M. K. Kaczmarek, H. Liu, F. Artizzu, L. D. Carlos and P. Van Der Voort, *Angew. Chem., Int. Ed.* **2020**, *59*, 1932-1940.
[8] Y. Kitagawa, M. Kumagai, P. P. Ferreira da Rosa, K. Fushimi and Y. Hasegawa, *Chem. – Eur. J.* **2021**, *27*, 264-269..
[9] A. N. Carneiro Neto, E. Mamontova, A. M. P. Botas, C. D. S. Brites, R. A. S. Ferreira, J. Rouquette, Y. Guari, J. Larionova, J. Long and L. D. Carlos, *Adv. Opt. Mater.* **2021**, *10*, 2101870.
[10] J.-C. G. Bünzli, *Coord. Chem. Rev.* **2015**, *293*, 19-47.
[11] S. Sato and M. Wada, *Bull. Chem. Soc. Jpn.*, **1970**, *43*, 1955-1962
[12] N. Sabbatini, M. Guardigli, I. Manet, F. Bolletta and R. Ziessel, *Inorg. Chem.* **1994**, *33*, 955-959.
[13] A. Beeby, D. Parker and J. A. G. Williams, *J. Chem. Soc., Perkin Trans.* **1996**, *2*, 1565-1579.
[14] S. Blair, R. Kataky and D. Parker, *New J. Chem.* **2002**, *26*, 530-535.
[15] G.-L. Law, R. Pal, L. O. Palsson, D. Parker and K.-L. Wong, *Chem. Commun.* **2009**, 7321-7323.
[16] J. Lehr, M. Tropiano, P. D. Beer, S. Faulkner and J. J. Davis, *Chem. Commun.* **2015**, *51*, 15944-15947.
[17] T. J. Sørensen, A. M. Kenwright and S. Faulkner, *Chem. Sci.* **2015**, *6*, 2054-2059.
[18] Y. Kitagawa, F. Suzue, T. Nakanishi, K. Fushimi, T. Seki, H. Ito and Y. Hasegawa, *Commun. Chem.* **2020**, 3, 3.
[19] Y. Kitagawa, M. Tsurui, and Y. Hasegawa, *RSC Adv.* **2022**, *12*, 810-821.
[20] S. Katagiri, Y. Tsukahara, Y. Hasegawa and Y. Wada, *Bull. Chem. Soc. Jpn.* **2007**, *80*, 1492-1503.
[21] M. Yamamoto, Y. Kitagawa, T. Nakanishi, K. Fushimi and Y. Hasegawa, *Chem. – Eur. J.* **2018**, *24*, 17719-17726.
[22] T_1 levels of *p*-dpb, Me-dpb, and *m*-dpb are estimated to be 27,200, 24,600, and 27,300 cm^{-1}, respectively, based on the phosphorescence measurements (Figure S19).
[23] D. Casanova, M. Llunell, P. Alemany and S. Alvarez, *Chem. – Eur. J.* **2005**, *11*, 1479-1494.
[24] Y. Hirai, T. Nakanishi, Y. Kitagawa, K. Fushimi, T. Seki, H. Ito and Y. Hasegawa, *Angew. Chem., Int. Ed.* **2017**, *56*, 7171-7175.
[25] A. V. Artem'ev, M. P. Davydova, A. S. Berezin, T. S. Sukhikh and D. G. Samsonenko, *Inorg. Chem. Front.* **2021**, *8*, 2261-2270.

23 [26] T_1 levels of *m*-dpf and *m*-dpc are estimated to be 23,000 and 27,700 cm^{-1}, respectively, based on the phosphorescence measurements (Figure S19).

Entry for the Table of Contents

Insert graphic for Table of Contents here.

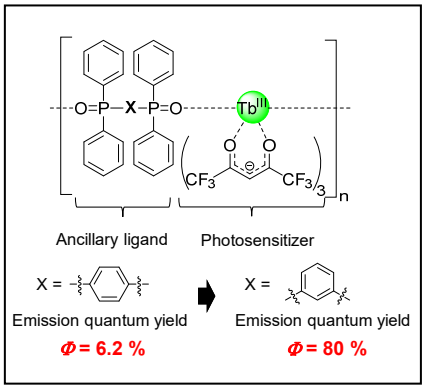

Molecular photosensitizers exhibit efficient light-absorbing capabilities in photo-functional materials. Herein, we report effective photosensitization at excited-state equilibrium using Tb^{III} coordination polymers. The coordination polymers are composed of Tb^{III} ions (as emission centers), hexafluoroacetylacetonate (as a photosensitizer ligand), and phosphine oxide-based bridges (as ancillary ligands). The ancillary ligand controls the excited state equilibrium between the photosensitizer and Tb^{III}, allowing the construction of Tb^{III} coordination polymer with high Tb^{III} emission quantum yield (≥ 70 %).

Institute and/or researcher Twitter usernames: